nature physics

Article

https://doi.org/10.1038/s41567-023-02221-1

Biofilms as self-shaping growing nematics

In the format provided by the authors and unedited

Supplementary Information for

Biofilms as self-shaping growing nematics

Supplementary Notes 1: Agent-based simulations

The agent-based simulations are built upon those developed in Nijjer *et al*.[1] and updated to include cell-gel adhesion. Briefly, we modelled the bacteria as spherocylinders that repelled each other through Hertzian mechanics and exhibited JKR-like adhesion to the glass substrate and confining gel. As cells moved parallelly relative to the substrate, they experienced a frictional force proportional to $\eta_{\mathrm{ABS}}\boldsymbol{v}$ where $\boldsymbol{v}$ was the velocity of the cells (driven by growth-induced expansion). The gel was modelled using a particle representation such that it exhibits linear elastic properties with stiffness E_{ABS} as well as adhesion to the glass substrate. The simulations began with a single cell which grew with a growth rate g and divided upon doubling in length. The simulation was stopped after 10 to 13 generations. The full details of the simulation are reported elsewhere[1,2] – here we only elaborate on the major updates regarding cell-cell interactions and cell-gel adhesion.

For cell-cell interactions, we neglect adhesion and friction between cells, and only consider elastic contacts between cells with a relatively stiff inner cell surrounded by a relatively soft extracellular matrix. We denote the radius of rigid cell (inner region) by R_{c} to differentiate it with the radius of cell-matrix composite R, and all the word "cell" represents "cell-matrix composite" in the following descriptions. We apply linear elastic Hertzian contact theory[3] to quantify the repulsive contact force on cell i by cell j, written as

$$\boldsymbol{F}_{\mathrm{cell-cell},ij}=\begin{cases}-\frac{5}{2}E_0R^{1/2}\delta_{ij}^{3/2}\hat{\mathbf{e}}_{ij}, \delta_{ij}<R-R_{\mathrm{c}}\\ -\frac{5}{2}(E_0R^{1/2}(R-R_{\mathrm{c}})^{3/2}+E_{\mathrm{c}}R^{1/2}\left(\delta_{ij}-R+R_{\mathrm{c}}\right)^{3/2})\hat{\mathbf{e}}_{ij}, \delta_{ij}>R-R_{\mathrm{c}}\end{cases}, \quad (1)$$

where E_0 and E_c denote the effective contact stiffness of the extracellular matrix and rigid cell respectively, δ_{ij} is the overlapping distance, and $\hat{\mathbf{e}}_{ij}$ denotes the unit vector obtained from normalizing the distance vector $\boldsymbol{d}$, defined as the smallest distance between two cell center lines. The overlapping distance δ_{ij} is given by $\delta_{ij} = 2R - |\boldsymbol{d}|$. Correspondingly, the moment about the cell center is given by

$$\boldsymbol{M}_{\text{cell}-\text{cell},ij} = s_{\text{r}}\hat{\boldsymbol{n}}_i \times \boldsymbol{F}_{\text{cell}-\text{cell},ij}, \tag{2}$$

where $\hat{\boldsymbol{n}}_i$ is the unit vector denoting cell orientation and s_{r} is the parametric coordinate of the contact point along the center line of the cell.

At the interface between the biofilm and the surrounding gel, we apply a JKR-type model to capture the elastic contact and adhesion between cell agents i and coarse-grained gel particles j. For the elastic contact, we use a similar linear elastic Hertzian contact interaction as in (1), written as

$$\boldsymbol{F}^{\text{rep}}_{\text{cell}-\text{gel},ij} = \begin{cases} -\frac{5}{2}E_0{R_{\text{eq}}}^{1/2}\delta_{ij}^{3/2}\hat{\mathbf{e}}_{ij}, \delta_{ij} < R - R_{\text{c}} \\ -\frac{5}{2}(E_0{R_{\text{eq}}}^{1/2}(R-R_{\text{c}})^{3/2} + E_{\text{c}}{R_{\text{eq}}}^{1/2}\left(\delta_{ij} - R + R_{\text{c}}\right)^{3/2})\hat{\mathbf{e}}_{ij}, \delta_{ij} > R - R_{\text{c}} \end{cases}, \tag{3}$$

where $R_{\text{eq}} = \frac{2R_{\text{gel}}R}{R+R_{\text{gel}}}$ is the equivalent radius of contact, R_{gel} is the radius of each coarse-grained gel particle, and the overlapping distance $\delta_{ij} = R + R_{\text{gel}} - |\boldsymbol{d}|$ is the minimal distance between the center of the gel particle to the cell center line.

We assume the adhesion force is proportional to $\gamma_{\mathrm{cell-gel}}$, the energy release per unit area given by $\gamma_{\mathrm{cell-gel}} = \gamma_{\mathrm{cell}} + \gamma_{\mathrm{gel}} - 2\gamma^*$, the surface energy of cell and gel minus twice the interfacial energy γ^*. Naturally, the adhesion force is also proportional to the contact area, which gives

$$\boldsymbol{F}^{\mathrm{adh}}_{\mathrm{cell-gel},ij} = \pi a^2 \gamma_{\mathrm{cell-gel}} \hat{\mathbf{e}}_{ij}, \tag{4}$$

where a is the equivalent radius of contact area, given by the simplified relation $a = \sqrt{\delta_{ij} R_{\mathrm{eq}}}$. For simplicity, our model neglects the cohesion-decohesion asymmetric behavior in the original JKR model, as the decohesion behavior is assumed to rarely happen on the continuously expanding biofilm-gel interface.

Similarly, the moment about the cell center, for the repulsive cell-gel contact force $\boldsymbol{F}^{\mathrm{rep}}_{\mathrm{cell-gel},ij}$ and the adhesion force $\boldsymbol{F}^{\mathrm{adh}}_{\mathrm{cell-gel},ij}$, can be given by

$$\boldsymbol{M}^{\mathrm{rep}}_{\mathrm{cell-gel},ij} = s_{\mathrm{r}} \widehat{\boldsymbol{n}}_i \times \boldsymbol{F}^{\mathrm{rep}}_{\mathrm{cell-gel},ij}, \tag{5}$$

and

$$\boldsymbol{M}^{\mathrm{adh}}_{\mathrm{cell-gel},ij} = s_{\mathrm{r}} \widehat{\boldsymbol{n}}_i \times \boldsymbol{F}^{\mathrm{adh}}_{\mathrm{cell-gel},ij}. \tag{6}$$

Supplementary Notes 2: Continuum modelling of morphogenesis of confined biofilms

Here we present a minimal model to explain the macroscopic morphogenesis of *V. cholerae* biofilms confined between an infinite elastic material and a hard substrate that are bonded together. As the biofilm grows, it induces elastic deformation in the surrounding gel, which can lead to delamination of the gel from the substrate. We assume the biofilm is axisymmetric and a schematic of the geometry is given in Extended Data Fig. 4.

We take the stiffness of the gel to be μ and assume an initial defect of radius r_i where the gel is initially not adhered to the substrate. We treat the growth of the biofilm as a quasistatic process and assume the gel is always in mechanical equilibrium. For a given biofilm volume V the biofilm has shape $r(z)$ with basal radius $r_\mathrm{b} \geq r_\mathrm{i}$; the elastic energy due to deformation of the gel is $U_\mathrm{e} = \mu r_\mathrm{b}^3 f\left(\frac{V}{r_\mathrm{b}^3}\right)$, where $f\left(\frac{V}{r_\mathrm{b}^3}\right)$ quantifies the elastic potential energy, which is only a function of the dimensionless volume V/r_b^3. There is no simple analytical form for f so we instead numerically determine it using the finite element software ABAQUS/CAE 2017[4]. The energy release due to breakage of gel-substrate bonds is $U_\mathrm{d} = \Gamma\pi(r_\mathrm{b}^2 - r_\mathrm{i}^2)$ with energy density Γ for $r_\mathrm{b} > r_\mathrm{i}$, and $U_\mathrm{d} = 0$ otherwise. Taking these two contributions together, the total energy of the system for $r_\mathrm{b} \geq r_\mathrm{i}$ is

$$U = U_\mathrm{d} + U_\mathrm{e} = \Gamma\pi\left(r_\mathrm{b}^2 - r_\mathrm{i}^2\right) + \mu r_\mathrm{b}^3 f\left(\frac{V}{r_\mathrm{b}^3}\right). \tag{7}$$

As the biofilm grows, it also experiences friction as cells are pushed along the substrate due to growth-induced motion. This is because the secreted adhesins bond the cells to the substrate, leading to frictional behavior as relative motion occurs[5]. We assume the frictional force is proportional to the velocity such that the friction experienced due to motion of a basal point on the biofilm is $\boldsymbol{F}_\mathrm{f} = \eta\boldsymbol{v}$, where $\boldsymbol{v}$ is the velocity of the biofilm at the substrate and η is the friction coefficient. The basal velocity is nearly axisymmetric and has little azimuthal component. Therefore, integrating over the whole basal area of the biofilm, the corresponding Rayleigh dissipation function is

$$D = \pi \int_0^{r_\mathrm{b}} \eta|\boldsymbol{v}|^2 r \, \mathrm{d}r. \tag{8}$$

In this case, we write $\boldsymbol{v} = v_r(r)\hat{r}$, and the velocity satisfies the condition $v_r(0) = 0$ and the kinematic condition $v_r(r_b) = \mathrm{d}r_\mathrm{b}/\mathrm{d}t$. We neglect energy dissipation in the bulk of the biofilm as the dissipation from growth along the substrate dominates[6,7]. Because the basal layer of the biofilm has a uniform density[1], mass conservation requires that the velocity satisfies

$$\frac{1}{r}\frac{\mathrm{d}(rv_r)}{\mathrm{d}r} = g', \tag{9}$$

where g' is the effective basal growth rate, which accounts for the loss and accumulation of biomass from the neighboring cells above and is not necessarily equal to the intrinsic biofilm growth rate g. Assuming g' is spatially uniform, and solving (9), we find

$$v_r = \frac{\mathrm{d}r_\mathrm{b}}{\mathrm{d}t}\frac{r}{r_\mathrm{b}}. \tag{10}$$

Note that in reality the velocity profile in the basal layer of WT* biofilms may deviate from this simple linear form[1]; however, the exact functional form does not affect the main conclusions of the current analysis. Substituting into (8), the Rayleigh dissipation function becomes

$$D = \frac{\pi\eta r_\mathrm{b}^2 \dot{r}_\mathrm{b}^{\,2}}{4} \tag{11}$$

where $\dot{r}_\mathrm{b} = \mathrm{d}r_\mathrm{b}/\mathrm{d}t$. Writing the Euler-Lagrange equation $\frac{\partial D}{\partial \dot{r}_\mathrm{b}} = -\frac{\partial U}{\partial r_\mathrm{b}}$ for the generalized basal radius coordinate r_b yields

$$\frac{\eta\pi r_\mathrm{b}^2}{2}\frac{\mathrm{d}r_\mathrm{b}}{\mathrm{d}t} = 3\mu r_\mathrm{b}^2\left(\frac{V}{r_\mathrm{b}^3}f'\left(V/r_\mathrm{b}^3\right) - f\left(V/r_\mathrm{b}^3\right)\right) - 2\Gamma\pi r_\mathrm{b}. \tag{12}$$

Using the fact that the whole biofilm grows exponentially ($\mathrm{d}V/\mathrm{d}t = gV$), we rewrite $\frac{\mathrm{d}r_\mathrm{b}}{\mathrm{d}t} = \frac{\mathrm{d}r_\mathrm{b}}{\mathrm{d}V} gV$. Substituting into (12) yields an ordinary differential equation for the evolution of the basal radius,

$$\frac{\eta\pi r_\mathrm{b}^2 gV}{2}\frac{\mathrm{d}r_b}{\mathrm{d}V} = 3\mu r_\mathrm{b}^2\left(\frac{V}{r_\mathrm{b}^3}f'\left(V/r_\mathrm{b}^3\right) - f\left(V/r_\mathrm{b}^3\right)\right) - 2\Gamma\pi r_\mathrm{b}, \tag{13}$$

which after non-dimensionalizing by the initial defect length-scale r_i becomes

$$\mathrm{H}\frac{\mathrm{d}\tilde{r}_\mathrm{b}}{\mathrm{d}\tilde{V}} = \mathrm{M}\frac{\tilde{F}\left(\tilde{V}/\tilde{r}_\mathrm{b}{}^3\right)}{\tilde{V}} - \frac{1}{\tilde{V}\tilde{r}_\mathrm{b}}, \tag{14}$$

where $\tilde{\cdot}$ denotes dimensionless quantities and $\tilde{F} = \frac{V}{r_\mathrm{b}^3}f'\left(V/r_\mathrm{b}^3\right) - f\left(V/r_\mathrm{b}^3\right)$. There are two key dimensionless variables: the dimensionless friction $\mathrm{H} = \eta g r_\mathrm{i}^2/4\Gamma$ and the dimensionless elastic modulus $\mathrm{M} = 3\mu r_\mathrm{i}/2\pi\Gamma$. Note that $\tilde{r}_\mathrm{b} \geq 1$ since r_b cannot shrink beyond the initial defect length; therefore, $\mathrm{d}\tilde{r}_\mathrm{b}/\mathrm{d}\tilde{V}$ is constrained to be larger than or equal to 0. We integrate (14) using a forward Euler method and we approximate the contact angle in the model from the unique spherical cap that has the same height $\tilde{z}_\mathrm{max}$ at $\tilde{r} = 0$ and same basal intercept $\tilde{r}_\mathrm{b}$.

To gain further insight into the model, we interrogate the potential dominant balances in (14). When the volume of the biofilm is small ($\tilde{V} \ll 1$), the lefthand term of (14) is negligible and the righthand two terms balance to give

$$\mathrm{M}\tilde{F}\left(\tilde{V}/\tilde{r}_\mathrm{b}{}^3\right)\tilde{r}_\mathrm{b} = 1. \tag{15}$$

Since $\tilde{r}_\mathrm{b}$ is constrained to be larger than 1, this balance leads to one of two behaviors: *interfacial cavitation* where the gel does not delaminate and $\tilde{r}_\mathrm{b} = 1$, or *delamination* where the gel continually detaches from the glass substrate and $\tilde{r}_\mathrm{b} > 1$. As the gel delaminates and $\tilde{r}_\mathrm{b}$ grows, when $\tilde{V}/{\tilde{r}_\mathrm{b}}^3 \ll 1$, $\tilde{F} \sim \left(\frac{\tilde{V}}{{\tilde{r}_\mathrm{b}}^3}\right)^2$, which means $\tilde{r}_\mathrm{b} \sim \tilde{V}^{2/5}$ and the biofilm becomes flatter over time. This scaling behavior is analogous to the scaling behavior observed in "toughness-dominated hydraulic fracture"[8,9] (note that this scaling law is consistent with the condition that $\tilde{V}/{\tilde{r}_\mathrm{b}}^3 \ll 1$ as volume increases). As the biofilm volume and radius grow, substrate friction becomes relatively important. For most physically relevant parameters, this eventually leads to a balance between friction and elastic deformation such that

$$\frac{\mathrm{H}}{\mathrm{M}}\frac{\mathrm{d}\tilde{r}_\mathrm{b}}{\mathrm{d}\tilde{V}} = \frac{\tilde{F}\left(\tilde{V}/{\tilde{r}_\mathrm{b}}^3\right)}{\tilde{V}}. \tag{16}$$

In this limit, the dynamics depend only on the ratio $\mathrm{H/M} = (\pi g r_\mathrm{i}/6)(\eta/\mu)$. Although the gel delaminates, the expansion of the delaminating interface is slowed by friction leading to *friction-limited delamination*. As the biofilm grows and the gel delaminates, when $\frac{\tilde{V}}{{\tilde{r}_\mathrm{b}}^3} \gg 1$, $\tilde{F} \sim \left(\frac{\tilde{V}}{{\tilde{r}_\mathrm{b}}^3}\right)^{1/2}$. In this limit, $\tilde{r}_\mathrm{b} \sim \tilde{V}^{1/5}$ and the biofilm becomes more dome-like over time (note that this scaling law is consistent with the condition that $\frac{\tilde{V}}{{\tilde{r}_\mathrm{b}}^3} \gg 1$ as volume increases). This regime is analogous to "viscous-dominated hydraulic fracture," albeit with different scaling laws[8–10]. These three regimes and the transition between them are summarized in Extended Data Figs. 4b and c.

We estimated the parameters in the model as follows:

Growth rate: The number of bacteria in a given biofilm was measured over time and the growth rate was found to be $g \approx 0.6\ \mathrm{hr}^{-1}$.

Gel modulus: The gel moduli as a function of agarose concentration were measured using shear rheometry and found to follow $\log \mu \approx 2.7 \log c + 9.4$ (Supplementary Figure 1).

Gel-substrate adhesion and initial defect size: We fit the contact angle transition as a function of both volume and gel modulus (for mature biofilms) for the non-adhesin-producing mutant. In this case, the mutant exhibits little substrate friction and therefore the contact angle transition is dominated by a balance between interfacial cavitation and delamination. Fitting yielded $r_\mathrm{i} \approx 5\ \mu\mathrm{m}$ and $\Gamma \approx 0.02\ \mathrm{N/m}$ (Ref. [4]).

Friction coefficient: In Beroz *et al.*[6], WT* *V. cholerae* cells were seeded in a microfluidic channel of cross-section $400 \times 60\ \mu\mathrm{m}^2$ and M9 media flowed through the channel at a rate of $500\ \mu\mathrm{L/min}$. They observed that the cells move at a rate of approximately $2\ \mu\mathrm{m/hr}$. The drag force on the cells can be approximated as that on a sphere and is $F = 6\pi R \eta_\mathrm{w} v_\mathrm{avg}$ where $R \approx 0.8\ \mu\mathrm{m}$ is the apparent radius of the cell, $\eta_\mathrm{w} \approx 8.9 \times 10^{-4}\ \mathrm{Pa\ s}$ is the viscosity of water and approximately that of the media, and $v_\mathrm{avg} \approx 0.35\ \mathrm{m/s}$ is the average fluid velocity in the channel. Taking the footprint of the cell as $A = 3\ \mu\mathrm{m}^2$, the substrate friction coefficient was estimated as $\eta = \frac{F}{A v_\mathrm{avg}} \approx 2 \times 10^{12}\ \mathrm{Pa\ s/m}$.

Limitation of the model: We note that while our model captures most of the features observed in the experiment, it does not predict a bifurcation in contact angle. The predicted change in the contact angle is smooth and no discrete jump in shape or bimodal distribution was predicted. Our current model assumes perfect material properties such as neo-Hookean response of the gel and no stick-slip behavior at the delaminating interface; however, in reality some of these assumptions may not hold. In particular, interfacial fracture (i.e. delamination) is known to be complex and

157 hysteretic[11], which may give rise to additional resistance to the initiation of delamination. The
158 bimodal distribution of contact angles may also be related to intrinsic randomness in adhesin
159 production.

160

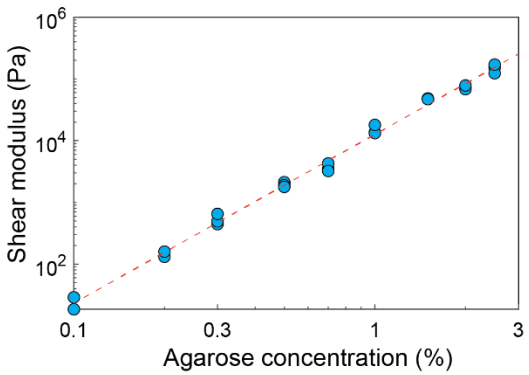

Supplementary Figure 1| Dependence of agarose gel stiffness on polymer concentration. Shear modulus μ as a function of the agarose concentration c. Each data point corresponds to a unique measurement from Zhang *et al.*[12] The dashed line corresponds to the line of best fit $\log \mu = 2.7 \log c + 9.4$.

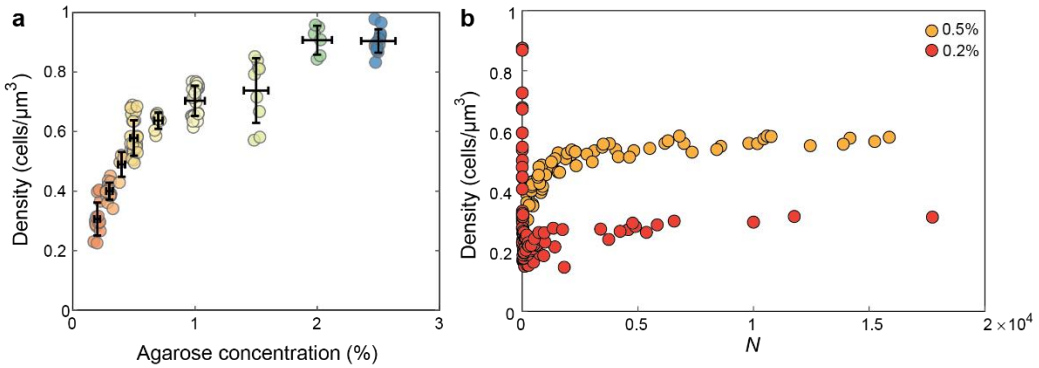

Supplementary Figure 2| Cell density as functions of agarose concentration and time. (a) Cell density of mature biofilms for different agarose concentrations (each dot denotes a unique biofilm). Vertical error bars correspond to mean ± s.d. in measurements and horizontal error bars correspond to uncertainty in agarose concentration. (**b**) Cell density as a function of the number of cells (*N*) for 4 and 8 biofilms measured over time at 0.2% and 0.5% agarose concentrations, respectively. In both cases, the density tends to a plateau instead of continually increasing, which suggests that the confining pressure tends to a constant rather than increasing unboundedly. This observation is consistent with the energetic model where the pressure in dome-shaped biofilms is predicted to tend to a constant value with increasing volume.

Supplementary Table 1: List of the strains used in this study

Strains	Genotype	Source
JN007	*vpvc*^{W240R}, Δ*vc1807::Ptac-mNeonGreen*-Spec^{R}	[1]
JN008	*vpvc*^{W240R}, Δ*rbmA,* Δ*vc1807::Ptac-mNeonGreen*-Spec^{R}	[1]
JY453	*vpvc*^{W240R}, Δ*rbmA,* Δ*vc1807::Ptac-SCFP3A*-Spec^{R}	This study
JN133	*vpvc*^{W240R}, Δ*rbmA,* Δ*vc1807::Ptac-mScarlet-I*-Spec^{R}	This study
JN036	*vpvc*^{W240R}, Δ*rbmA,* Δ*bap1,* Δ*rbmC,* Δ*vc1807::Ptac-mNeonGreen*-Spec^{R}, pJY057	[1]
JN148	*vpvc*^{W240R}, Δ*rbmA,* Δ*lacZ::Ptac-mNeonGreen-µNS,* Δ*vc1807::Ptac-mScarlet-I*-Spec^{R}	[1]
JN150	*Vpvc*^{W240R}, Δ*rbmA,* Δ*bap1,* Δ*rbmC,* Δ*lacZ::Ptac-mNeonGreen-µNS,* Δ*vc1807::Ptac-mScarlet-I*-Spec^{R}	[1]
JN151	*vpvc*^{W240R}, Δ*vpsL,* Δ*lacZ::Ptac-mNeonGreen-µNS,* Δ*vc1807::Ptac-mScarlet-I*-Spec^{R}	This study
Plasmid		
pJY057	Kan^{R}, *araC-*P_{BAD}*-bap1*	[13]

Supplementary references:

1. Nijjer, J. *et al.* Mechanical forces drive a reorientation cascade leading to biofilm self-patterning. *Nat. Commun.* **12**, 6632 (2021).

2. Li, C. *et al.* Mechano-lithography: stress anisotropy driven nematic order in growing three-dimensional bacterial biofilms. Preprint at https://doi.org/10.48550/arXiv.2211.16354 (2022).

3. Willis, J. R. Hertzian contact of anisotropic bodies. *J. Mech. Phys. Solids* **14**, 163–176 (1966).

4. Henzel, T. *et al.* Interfacial cavitation. *PNAS Nexus* **1**, pgac217 (2022).

5. Fei, C. *et al.* Nonuniform growth and surface friction determine bacterial biofilm morphology on soft substrates. *Proc. Natl. Acad. Sci. USA* **117**, 7622–7632 (2020).

6. Beroz, F. *et al.* Verticalization of bacterial biofilms. *Nat. Phys.* **14**, 954–960 (2018).

7. Zhang, Q. *et al.* Mechanical resilience of biofilms toward environmental perturbations mediated by extracellular matrix. *Adv. Funct. Mater.* **32**, 2110699 (2022).

8. O'Keeffe, N. J., Huppert, H. E. & Linden, P. F. Experimental exploration of fluid-driven cracks in brittle hydrogels. *J. Fluid Mech.* **844**, 435–458 (2018).

9. Lai, C.-Y., Zheng, Z., Dressaire, E. & Stone, H. A. Fluid-driven cracks in an elastic matrix in the toughness-dominated limit. *Philos. Trans. Royal Soc. A* **374**, 20150425 (2016).

10. Lai, C.-Y., Zheng, Z., Dressaire, E., Wexler, J. S. & Stone, H. A. Experimental study on penny-shaped fluid-driven cracks in an elastic matrix. *Philos. Trans. Royal Soc. A* **471**, 20150255 (2015).

11. Creton, C. & Ciccotti, M. Fracture and adhesion of soft materials: a review. *Rep. Prog. Phys.* **79**, 046601 (2016).

12. Zhang, Q. *et al.* Morphogenesis and cell ordering in confined bacterial biofilms. *Proc. Natl. Acad. Sci. USA* **118**, e2107107118 (2021).

13. Yan, J., Sharo, A. G., Stone, H. A., Wingreen, N. S. & Bassler, B. L. *Vibrio cholerae* biofilm growth program and architecture revealed by single-cell live imaging. *Proc. Natl. Acad. Sci. USA* **113**, e5337-5343 (2016).